Angular Distribution of Single-Quantum Annihilation Radiation*

W. R. JOHNSON
University of Notre Dame, Notre Dame, Indiana
(Received 16 January 1967)

Angular distributions of radiation accompanying single-quantum annihilation of positrons by K-shell electrons are calculated. These angular distributions differ from the corresponding Born-approximation calculations, both in magnitude and in shape. For transversely polarized positrons the radiation exhibits an azimuthal asymmetry. The asymmetry, together with the spin-independent part of the differential cross section, is presented for various elements ranging from $Z=47$ to $Z=92$. Because of the relatively large magnitude of the asymmetry for high-Z targets, it is suggested that detection of the radiation caused by positrons, transversely polarized by an electrostatic analyzer, could provide an alternative means for measuring the longitudinal polarization of positrons emitted in nuclear β-decay. Total cross sections obtained by numerically integrating the angular distributions agree precisely with a previous total-cross-secton calculation and serve as a measure of the accuracy of the present results.

I. INTRODUCTION

THE possibility of single-quantum annihilation (S.Q.A.) of positrons with bound atomic electrons has been known for many years.[1–3] Only recently, however, has experimental attention been drawn to this process because of the technical difficulty of separating single-quantum annihilation radiation from the background radiation. In the past few years several experimenters[4–6] have been able to detect single-quantum annihilation radiation from positrons annihilating in atomic K shells and to measure the Z dependence of the total cross section. These measurements are in agreement with previous calculations of the total cross section made using relativistic Coulomb wave functions for both the K-shell electron and the incident positron.[3,7]

The only existing theoretical angular distributions are those obtained from the Born approximation.[2] Since the total cross sections predicted by the Born approximation are known to be in error by factors greater than 2 for high-Z elements it is necessary to re-evaluate the angular distributions using relativistic Coulomb wave functions to obtain reliable theoretical predictions.

The incident positrons are scattered by the nucleus before annihilating with the K-shell electron. If these positrons are transversely polarized the scattering will exhibit a left-right asymmetry with respect to the plane defined by the positron spin and momentum vectors. This left-right scattering asymmetry reflects a corresponding asymmetry in the annihilation radiation. Of course in a Born-approximation calculation where the incident positron is described by a plane wave no asymmetry appears.

Measurement of the asymmetry, which is appreciable for high-Z elements, should provide a useful tool for detecting transverse polarization of positrons. These measurements could also serve to detect longitudinal polarization by passing positrons from a radioactive source through a 90° electrostatic deflector before allowing them to annihilate, as illustrated schematically in Fig. 1. In this way, the asymmetry measurement could provide a useful alternative to Bhabha scattering[8] as a technique for positron polarization measurements. Similar techniques have been applied successfully to obtain electron polarization from Mott-scattering asymmetry.[9,10]

The angular distribution peaks sharply in the forward direction, for the elements and energies considered here, and falls off rapidly at backward angles. This behavior is in conflict with the Born approximation, which predicts an angular distribution vanishing at both forward and backward angles. The asymmetry maximizes for positron kinetic energies in the 200–400 keV range and has the same sign as the corresponding Coulomb scattering asymmetry. The spin-dependent part of the cross section maximizes for angles in the 30°–60° range.

II. DIFFERENTIAL CROSS SECTION

The single-quantum annihilation differential cross section is given by

$$d\sigma/d\Omega=(\alpha/2\pi)\,(E\omega/p)\sum_{\epsilon,\mu}|\,T\,|^2, \qquad (1)$$

* Work supported in part by the U.S. Atomic Energy Commission.

[1] E. Fermi and G. E. Uhlenbeck, Phys. Rev. **44**, 510 (1933).
[2] H. J. Bhabha and H. R. Hulme, Proc. Roy. Soc. (London) **A146**, 723 (1934).
[3] J. C. Jaeger and H. R. Hulme, Proc. Cambridge Phil. Soc. **32**, 158 (1936).
[4] L. Sodickson, W. Bowman, J. Stephenson, and R. Weinstein, Phys. Rev. **124**, 1851 (1961).
[5] H. Langhoff, H. Weigmann, and A. Flammersfeld, Nucl. Phys. **41**, 575 (1963).
[6] H. Weigmann, H. Hansen, and A. Flammersfeld, Nucl. Phys. **45**, 555 (1963).
[7] W. R. Johnson, D. J. Buss, and C. O. Carroll, Phys. Rev. **135**, A1232 (1964).
[8] *Beta- and Gamma-Ray Spectroscopy*, edited by K. Siegbahn (North-Holland Publishing Company, Amsterdam, 1965), Vol. II, Chaps. XXIII, XXIV.
[9] J. S. Greenberg and D. M. Lazarus, in Proceedings of the International Conference on Weak Interactions, 1965, Argonne National Laboratory Report ANL-7130, p. 313, (unpublished).
[10] J. S. Greenberg, D. P. Malone, R. L. Gluckstern, and V. W. Hughes, Phys. Rev. **120**, 1393 (1960).

where the T matrix element is

$$T=\int d^3r[v_s^\dagger(\mathbf{r})\,\boldsymbol{\alpha}\cdot\hat{\epsilon}u_\mu(\mathbf{r})]\exp(-i\mathbf{k}\cdot\mathbf{r}). \quad (2)$$

We denote the energy-momentum vectors of the positron and photon by $(\mathbf{p}, iE)$ and $(\mathbf{k}, i\omega)$, and use $\hat{\epsilon}$ for the photon-polarization vector. The Coulomb-field Dirac wave functions $v_s(\mathbf{r})$ and $u_\mu(\mathbf{r})$ describe a positron with spin s and a K-shell electron with magnetic quantum number μ. We sum over photon-polarization states and magnetic quantum numbers in Eq. (1) but leave the positron spin direction arbitrary.

The K-shell wave function is given by

$$u_\mu(\mathbf{r})=\begin{pmatrix} ig_{-1}(\lambda r)\Omega_{-1\mu}(\hat{r}) \\ f_{-1}(\lambda r)\Omega_{1\mu}(\hat{r})\end{pmatrix}, \qquad \mu=\pm\tfrac{1}{2}, \quad (3)$$

and the positron wave function by

$$v_s(\mathbf{r})=4\pi\sum_{\kappa,m}P_{\kappa m}(\mathbf{p},s)\exp[-i\delta_\kappa'-i(l-1)\pi/2]\times\begin{pmatrix} f_\kappa(pr)\Omega_{\kappa m}(\hat{r}) \\ -ig_\kappa(pr)\Omega_{-\kappa m}(\hat{r})\end{pmatrix},$$

$$P_{\kappa m}(\mathbf{p},s)=(-1)^{s-1/2}(\Omega_{\kappa m}^\dagger(\mathbf{p})\chi_{-s}),$$

$$\delta_\kappa'=\delta_\kappa+(l+1)\pi/2. \quad (4)$$

Here $\kappa=\mp(j+\frac{1}{2})$ for $j=l\pm\frac{1}{2}$ and δ_κ is the positron-scattering phase shift.

The spin angular function $\Omega_{\kappa m}(\hat{r})$ and the radial functions f_κ and g_κ for both the K-shell electron and the positron are known in analytic form for a Coulomb field.[11,12] We normalize the positron wave function by requiring that asymptotically it approach a plane wave with a spherical incoming wave.[13]

We choose the direction of the outgoing photon as z axis and perform the angular integrals in Eq. (2). Similar reductions are familiar from the theory of the atomic photoeffect.[14,15] The T matrix element is thereby reduced to

$$T=-4\pi i\sum_\kappa P_{\kappa,\mu+1}{}^*R_\kappa^+(\mu)\epsilon_+{}^*+P_{\kappa,\mu-1}{}^*R_\kappa^-(\mu)\epsilon_-{}^*, \quad (5)$$

where $\epsilon_\pm=\epsilon_x\pm i\epsilon_y$. The spin functions $P_{\kappa,m}$ are given in Eq. (4), while $R_\kappa^\pm(\mu)$ are finite sums of radial integrals given by

$$R_\kappa^+(\tfrac{1}{2})=[l(l+1)]^{1/2}\times[(l-1)^{1/2}\delta_{j,l-1/2}-(l+2)^{1/2}\delta_{j,l+1/2}]D_\kappa,$$

$$R_\kappa^-(\tfrac{1}{2})=-[l^{1/2}\delta_{j,l-1/2}+(l+1)^{1/2}\delta_{j,l+1/2}]S_\kappa, \quad (6)$$

$$R_\kappa^\pm(-\tfrac{1}{2})=-\mathrm{sign}(\kappa)R_\kappa^\mp(\tfrac{1}{2}).$$

Here we have used

$$D_\kappa=(2l'+1)^{-1}(I_{\kappa,l'-1}-I_{\kappa,l'+1}), \quad (7)$$

$$S_\kappa=J_{\kappa,l}+(2l'+1)^{-1}(l'I_{\kappa,l'-1}+(l'+1)I_{\kappa,l'+1}).$$

In Eqs. (6) and (7), l is the "orbital" angular momentum of a positron partial wave and $l'=2j-l$. The radial integrals $I_{\kappa l_1}$ and $J_{\kappa l_1}$ appearing in Eqs. (7) are given by

$$I_{\kappa l_1}=i^{(l-l_1)}\exp(i\delta_\kappa')\int_0^\infty r^2f_\kappa(pr)f_{-1}(\lambda r)j_{l_1}(kr)\,dr,$$

$$J_{\kappa l_1}=i^{(l-l_1)}\exp(i\delta_\kappa')\int_0^\infty r^2g_\kappa(pr)g_{-1}(\lambda r)j_{l_1}(kr)\,dr. \quad (8)$$

These radial integrals are the complex conjugates of i times the corresponding integrals given in Ref. 7.

We introduce four production amplitudes defined by

$$G_\pm=(4\pi)^{1/2}\sum_\kappa C(l,\tfrac{1}{2},j;\pm1,\tfrac{1}{2})R_\kappa^\pm(\tfrac{1}{2})Y_l{}^{\pm1}(\theta,\phi),$$

$$F_\pm=(4\pi)^{1/2}\sum_\kappa C(l,\tfrac{1}{2},j;l\pm1,-\tfrac{1}{2})R_\kappa^\pm(\tfrac{1}{2})Y_l{}^{l\pm1}(\theta,\phi). \quad (9)$$

The Clebsch–Gordan coefficients in Eqs. (9) are evaluated in terms of l and the spherical harmonics reduced to derivatives of Legendre polynomials (we choose $\mathbf{p}$ in the x–z plane). The amplitudes $F_\pm$ and $G_\pm$ become

$$G_+=\sin\theta\sum_{l=1}^\infty[(l+2)D_{-l-1}+(l-1)D_l]P_l'(\cos\theta),$$

$$F_+=\sin^2\theta\sum_{l=2}^\infty(D_l-D_{-l-1})P_l''(\cos\theta),$$

$$G_-=\sin\theta\sum_{l=1}^\infty(S_l-S_{-l-1})P_l'(\cos\theta),$$

$$F_-=-\sum_{l=0}^\infty[(l+1)S_{-l-1}+lS_l]P_l(\cos\theta), \quad (10)$$

with S_κ and D_κ given in Eqs. (7).

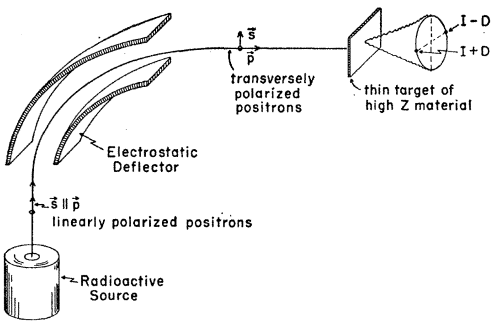

FIG. 1. Schematic arrangement for detecting longitudinal polarization of positrons using thin-target S.Q.A. I and D are the angular distribution and asymmetry functions of Eq. (11).

[11] M. E. Rose, *Relativistic Electron Theory* (John Wiley & Sons, Inc., New York, 1961), Chap. V.

[12] M. E. Rose, *Elementary Theory of Angular Momentum* (John Wiley & Sons, Inc., New York, 1957), Chap. IX.

[13] The wave function chosen here has the asymptotic form

$$\exp[-i\mathbf{p}\cdot\mathbf{r}-iv\ln(pr-\mathbf{p}\cdot\mathbf{r})]v_s(\mathbf{p})+F_s(r)\exp[-ipr+iv\ln(2pr)]/r,$$

where $v_s(\mathbf{p})$ is a positron bi-spinor. This is the wave function appropriate to an "in" scattering state; it disagrees with the choice made in Ref. 7. The alternative choice, appropriate to an "out" scattering state, leaves the differential cross section unchanged, but changes the sign of the asymmetry. Total cross sections, computed with either choice, will obviously agree.

[14] R. H. Pratt, R. D. Levee, R. L. Pexton, and W. Aron, Phys. Rev. **134**, A898 (1964).

[15] J. J. Matese and W. R. Johnson, Phys. Rev. **140**, A1 (1965).

The T matrix element in Eq. (5) can be expressed in terms of the production amplitudes and the sum over photon polarizations and electron magnetic quantum numbers can be carried out. The differential cross section reduces to

$$d\sigma/d\Omega = I(\theta) + \mathbf{n}\cdot\mathbf{s}D(\theta), \tag{11}$$

where $\mathbf{n}=\mathbf{k}\times\mathbf{p}/|\mathbf{k}\times\mathbf{p}|$ is the unit normal to the production plane, and $\mathbf{s}$ is the positron spin direction (referred to the positron rest frame). The functions $I(\theta)$ and $D(\theta)$ are determined from the amplitudes $F_\pm$ and $G_\pm$ by the relations

$$I(\theta) = 4\alpha(E\omega/p)\,(|G_+|^2+|F_+|^2+|G_-|^2+|F_-|^2), \tag{12}$$

$$D(\theta) = 8\alpha(E\omega/p)\ \mathrm{Im}(F_+^*G_+ + F_-^*G_-).$$

III. RADIAL INTEGRALS

The integrals $I_{\kappa l_1}$ and $J_{\kappa l_1}$ are simply related to the corresponding integrals of Ref. 7. However, because of certain difficulties which arise when the technique of Ref. 7 is used for large values of $|\kappa|$ and l_1, it was decided to use an alternative method to evaluate the integrals, whereby the accuracy could be carefully controlled.[16]

Integration Technique

The integrals were evaluated using an 11th-order closed-type Newton-Cotes formula:

$$\int_{x_0}^{x_8} f(x)\,dx = \frac{4h}{14175}\,(989f_0+5888f_1-928f_2+10496f_3 - 4540f_4+10496f_5-928f_6+5888f_7+989f_8) - (2368/467775)f^{(10)}(\xi)h^{11}. \tag{13}$$

Step sizes h were chosen as $\pi/12k$, $\pi/24k$, and $\pi/48k$, where $k=\omega$ is the photon wave number. The choice of a fraction of π/k was dictated by the asymptotic behavior of the most rapidly varying factor in Eqs. (8), $j_l(kr)$. As a guide to the accuracy to be expected using this method choose $h=\pi/24k$ and apply Eq. (13) to the integral

$$I=\int_0^\pi \sin kx\,dx = 2/k. \tag{14}$$

An upper bound on the error term in Eq. (13) is $3\times(2368/467775)\,(hk)^{11}/k$. Setting $h=\pi/24k$, we find a bound on the relative error $\Delta I/I<1.5\times10^{-12}$. If we use step size $\pi/12k$ the error will be increased by a factor of approximately 2^{11}, giving a relative error of less than 3.0×10^{-9}. Both of these values are less than the 7.4×10^{-9} truncation error of floating-point numbers in a 36-bit digital computer.

The integrals evaluated in this computation have an infinite upper limit. A practical upper limit was taken to be $R_{\max}=20/m\alpha Z$ so that the bound-state factor $\exp(-m\alpha Z r)$ is reduced by a factor $e^{-20}\sim 2.0\times10^{-9}$ from its maximum value. There is of course a problem involved here since the continuum wave function will be increasing at $R_{\max}$ unless $R_{\max}>(l+\frac{1}{2})/p$. We place an upper limit on the number of angular momentum states $l_{\max}\leq 20$, and consider energies $E\geq 1.25m$ ($p\geq 0.75m$): then even for the heaviest element considered ($Z=92$), $(l_{\max}+\frac{1}{2})/p_{\min}<R_{\max}$. The endpoint $R_{\max}$ is therefore in the oscillating region of both the continuum wave function and the spherical Bessel function.

As a realistic test of the above considerations we used the integration procedure to evaluate numerically:

$$\int_0^\infty r^2 j_l(kr) j_l(pr)\,\exp(-m\alpha Z r)\,dr = -\frac{m\alpha Z}{p^2k^2}\,Q_l'\left(\frac{E}{p}\right), \tag{15}$$

where $Q_l'(x)$ is the first derivative of a Legendre function of the second kind. For a range of energies $1.25m$ to $2.00m$ and for values of αZ from 0.2 to 0.8, numerical evaluation gave values of these test integrals of relative accuracy better than 1 part in 10^6 for $0\leq l\leq 20$. The limitation on accuracy is the error due to partial cancellation of the cyclic terms in the integrand.

Continuum Wave Functions

The continuum wave functions $f_\kappa(pr)$ and $g_\kappa(pr)$ were generated by solving the radial Dirac equations

$$\frac{df_\kappa}{dr}+\frac{(1-\kappa)}{r}f_\kappa-\left(E-m-\frac{\alpha Z}{r}\right)g_\kappa=0,$$
$$\frac{dg_\kappa}{dr}+\frac{(1+\kappa)}{r}g_\kappa+\left(E+m-\frac{\alpha Z}{r}\right)f_\kappa=0. \tag{16}$$

We use a ninth-order predict-correct system based on an open-type Newton–Cotes predictor:

$$y_8 = y_0+(8h/945)\,(460y_7'-954y_6'+2196y_5'-2459y_4' +2196y_3'-954y_2'+460y_1')+(3956/14175)\,y^{(9)}(\xi)h^9, \tag{17}$$

where y represents either f_κ or g_κ. As is well known, this type of finite-difference technique has inherent instabilities due to the occurrence of extraneous roots in the "indicial" equation. These instabilities are resolved by using the predicted value of y_8 to evaluate y_8', and by substituting this value into a stable "Adam's"-type corrector of ninth order:

$$y_8 = y_7+(h/120960)\,(36799y_8'+139849y_7'-121797y_6' +123133y_5'-88547y_4'+41499y_3'-11351y_2'+1375y_1') - (33953/3628800)\,y^{(9)}(\xi)h^9. \tag{18}$$

Equation (18) is iterated until the predicted and corrected values of y_8 agree to 1 part in 10^7. This iteration is only rarely necessary because the predicted value from Eq. (17) is usually within 10^{-7} of the corrected value. When this convergence criterion is satisfied the

[16] These difficulties were pointed out to the author by Dr. L. C. Maximon.

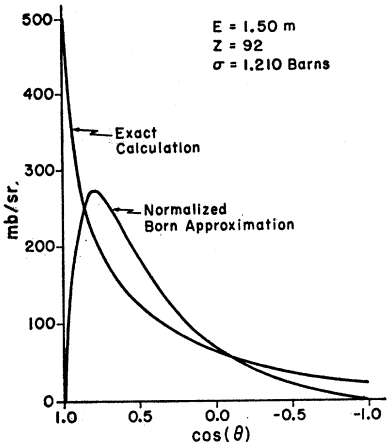

FIG. 2. Comparison of the Born-approximation angular distribution (normalized to give the correct total cross section) with the exact angular distribution for Uranium $Z=92$ at incident positron energy $E=1.5m$.

predictor is used to obtain an estimate of y at the next point and the cycle is repeated.

To get some idea of the error for each application of Eqs. (17) and (18) consider $y(x)=\sin px$. For the predictor formula we find

$$\text{Error}\approx\tfrac{1}{3}(ph)^9\approx 2\times10^{-10} \quad \text{for} \quad h=\pi/24k,$$
$$\approx 1\times10^{-7} \quad \text{for} \quad h=\pi/12k,$$

while for the corrector formula we have

$$\text{Error}\approx\tfrac{1}{100}(ph)^9\approx 6\times10^{-12} \quad \text{for} \quad h=\pi/24k,$$
$$\approx 3\times10^{-9} \quad \text{for} \quad h=\pi/12k.$$

We have used the fact above that $p/k\leq 1/\sqrt{2}$ for $E\leq 2.0m$. The theoretical error limitations will not be obtained of course since the corrector cycle will be discontinued when the predicted and corrected values at a given point agree to within 1 part in 10^7. A more realistic error limitation is thus simply 1×10^{-7}.

Mention must be made of how the first few values of y are generated to start the predict-correct cycle. It is easily seen that errors in the initial values of y propagate roughly as $(1+(|\kappa|+1)h/r)$, where r is some mean initial radius. To reduce the $(|\kappa|+1)h/r$ term compared with 1 we choose the initial value of r to be $5(|\kappa|+1)h$; the error propagation factor is then 1.2, and initial errors will be only moderately amplified.

The values of $f_\kappa(pr)$ and $g_\kappa(pr)$ at the points $0\leq r\leq 5(|\kappa|+1)h$ are computed using the power series representation of the Dirac functions:

$$g_\kappa(pr)=\sum_{n=0}^{\infty} a_n r^{n+\gamma}, \qquad f_\kappa(pr)=\sum_{n=0}^{\infty} b_n r^{n+\gamma}, \quad (19)$$

where $\gamma=[\kappa^2-(\alpha Z)^2]^{1/2}$, and where a_n and b_n are determined by the recurrence relations

$$a_{n+1}=\frac{(E-m)\alpha Z a_n-(E+m)(n+1+\gamma-\kappa)b_n}{(n+1)(n+1+2\gamma)},$$
$$b_{n+1}=\frac{(E-m)(n+1+\gamma+\kappa)a_n+(E+m)\alpha Z b_n}{(n+1)(n+1+2\gamma)}. \quad (20)$$

The initial values of a_n and b_n are chosen according to

$$b_0=\left(\frac{E-m}{2E}\right)^{1/2}\exp[-\tfrac{1}{2}(\nu\pi)]\,\frac{|\Gamma(\gamma-i\nu)|}{\Gamma(2\gamma+1)}\times(2p)^{\gamma-1}2(\gamma\sin\eta-\nu\cos\eta),$$
$$a_0=[\alpha Z/(\gamma+\kappa)]b_0,$$
$$\eta=\tfrac{1}{2}\tan^{-1}[(\kappa\nu+\gamma\nu')/(\gamma\kappa-\nu\nu')]-\tfrac{1}{2}\pi, \quad \text{for } \kappa>0; \quad (21)$$

and

$$a_0=\left(\frac{E+m}{2E}\right)^{1/2}\exp[-\tfrac{1}{2}(\nu\pi)]\,\frac{|\Gamma(\gamma-i\nu)|}{\Gamma(2\gamma+1)}\times(2p)^{\gamma-1}2(\gamma\cos\eta+\nu\sin\eta),$$
$$b_0=[\alpha Z/(\gamma-\kappa)]a_0,$$
$$\eta=\tfrac{1}{2}\tan^{-1}[(\kappa\nu+\gamma\nu')/(\gamma\kappa-\nu\nu')], \quad \text{for} \quad \kappa<0. \quad (22)$$

In Eqs. (21) and (22) $\nu=\alpha ZE/p$ and $\nu'=\alpha Zm/p$. The values for a_0 and b_0 are chosen so that asymptotically

$$g_\kappa(pr)\to[(E+m)/2E]^{1/2}[\cos(pr+\delta_\kappa)/pr],$$
and (23)
$$f_\kappa(pr)\to[(E-m)/2E]^{1/2}[\sin(pr+\delta_\kappa)/pr],$$

where the positron-scattering phase shift

$$\delta_\kappa=\eta-\tfrac{1}{2}\pi\gamma-\arg\Gamma(\gamma-i\nu). \quad (24)$$

As a practical test of the accuracy of the predict-correct routines we chose $\alpha Z=0$ and generated spherical Bessel functions. These Bessel functions were accurate to better than 1 part in 10^6 for E between $1.25m$ and

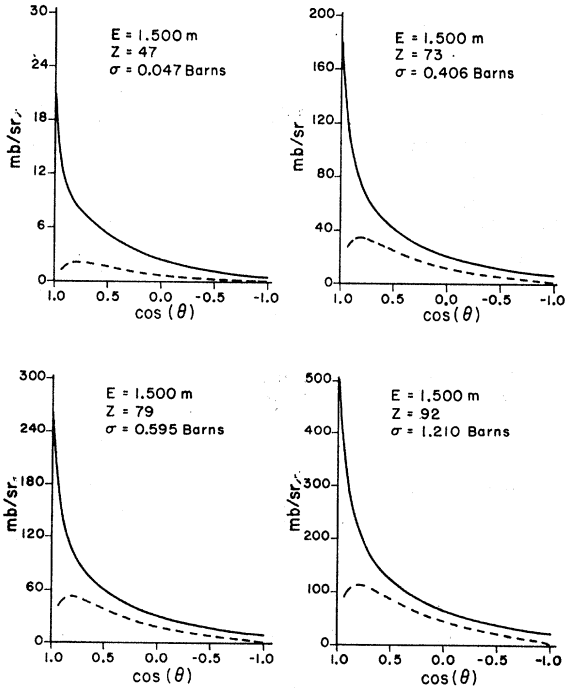

FIG. 3. Angular distribution functions $I(\theta)$ and asymmetry functions $D(\theta)$ for $E=1.5m$ and $Z=47$, 73, 79, 92. The solid curves represent $I(\theta)$ and the dashed curves represent $D(\theta)$.

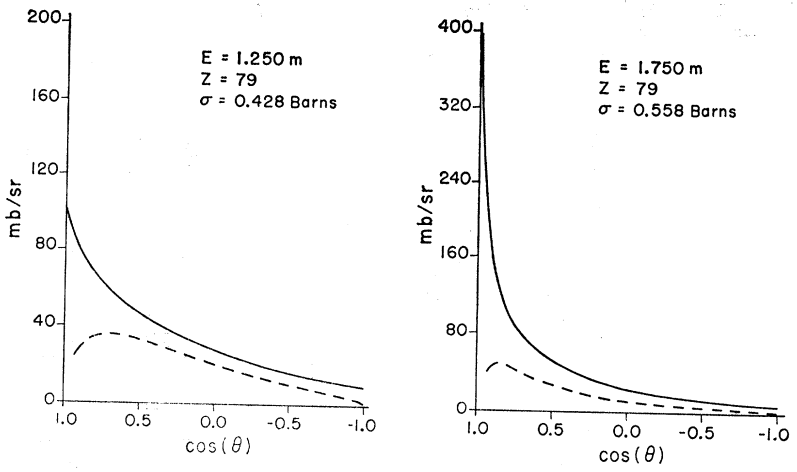

FIG. 4. Angular distribution functions $I(\theta)$ and asymmetry functions $D(\theta)$ for gold $Z=79$, at incident positron energies $E=1.25m$ and $1.75m$. The solid curves represent $I(\theta)$ and the dashed curves represent $D(\theta)$.

$2.00m$ and for values of $\kappa=\pm1, \pm10, \pm20$. We conclude that 1 part in 10^6 should be a reliable measure of the error of the continuum Coulomb wave functions.

Bound-State Wave Functions and Spherical Bessel Functions

The bound-state wave functions

$$g_{-1}(\lambda r)=N[\tfrac{1}{2}(1+\gamma_1)]^{1/2}r^{\gamma_1-1}e^{-\lambda r}, \qquad (25)$$
$$f_{-1}(\lambda r)=N[\tfrac{1}{2}(1-\gamma_1)]^{1/2}r^{\gamma_1-1}e^{-\lambda r},$$

with $N=[(2\lambda)^{2\gamma_1+1}/\Gamma(2\gamma_1+1)]^{1/2}$, $\gamma_1=[1-(\alpha Z)^2]^{1/2}$, and $\lambda=m\alpha Z$, are generated directly using Eqs. (25). The spherical Bessel functions $j_l(kr)$ occurring in Eqs. (8) are generated using recurrence relations. In the oscillating region $x>l+\frac{1}{2}$, $j_l(x)$ is generated using upward recurrence relations, while in the monotone region $x<l+\frac{1}{2}$, $j_l(x)$ is determined from arbitrarily assigned initial values using downward recurrence relations as suggested by Miller.[17]

The numerical values generated in this way agreed with tabulated values to 1 part in 10^7 for the range of parameters relevant to this problem.

Considering the accuracy of the various parts of the calculation described above it is believed that the final numerical values for the integrals $I_{\kappa l}$ and $J_{\kappa l}$ are of relative accuracy better than 1 part in 10^5.

In Table I selected values of the differential cross section $I(\theta)$ generated using the numerical procedure described above are compared with the values obtained using the technique of Ref. 7. These values appear to be consistent to the accuracy quoted above. The difficulties with the techniques of Ref. 7 mentioned at the beginning of this section are seen to be unimportant for the energies considered here. It is clear that the numerical methods above can be applied with some modification to the calculation of the (small) effects of atomic screening by using a suitable screened potential rather than $V(r)=\alpha Z/r$.

TABLE I. Comparison of the angular distribution function $I(\theta)$ at various angles for $Z=47$ and $Z=92$. The columns labeled $h=\pi/24k$ and $h=\pi/48k$ were computed using the method of Sec. III with the indicated step sizes. The columns labeled (a) were evaluated using the radial integrals from Ref. 7.

	$Z=47$		$Z=92$	
$\cos\theta$	$h=\pi/24k$	(a)	$h=\pi/48k$	(a)
1.0	20.4823	20.4827	496.404	496.401
0.5	5.30892	5.30892	122.874	122.874
0	2.38959	2.38958	64.2778	64.2775
−0.5	1.09834	1.09832	36.8700	36.8696
−1.0	0.473948	0.473920	21.9782	21.9779

[17] *Handbook of Mathematical Functions*, edited by M. Abramowitz and I. A. Stegun (U. S. Department of Commerce, National Bureau of Standards Washington, D. C., 1964), Appl. Math Series 55, Chap. X.

IV. RESULTS AND CONCLUSIONS

The radial integrals $I_{\kappa l}$ and $J_{\kappa l}$ were combined to form the parameters D_κ and S_κ of Eqs. (7). These parameters were then used together with the appropriate Legendre functions to evaluate the amplitude $F_\pm$ and $G_\pm$ in Eqs. (10). The partial-wave sums were evaluated using both 10 and 20 terms ($|\kappa|\leq10$, $|\kappa|\leq20$). The additional 10 partial waves changed the amplitudes and the total cross section by less than 0.1%. The angular distribution $I(\theta)$ and asymmetry function $D(\theta)$ were determined by combining the amplitudes according to Eqs. (12).

As a further check on the accuracy of the calculations, the function $I(\theta)$ was integrated numerically and the total cross section compared with the results of the direct calculations of Ref. 7. The two calculations agreed precisely to the three significant figures quoted in Table I of that reference.

The Born-approximation[2] angular distribution

$$\frac{d\sigma}{d\Omega}=\alpha^4Z^5r_0^2\,\frac{m^4p}{E^3k^2}\,\frac{\sin^2\theta}{(1-\beta\cos\theta)^3}$$
$$\times\left(\frac{E}{m}+2-\frac{2m^2}{Ek(1-\beta\cos\theta)}\right), \qquad (26)$$

where $r_0=$electron radius, and $\beta=p/E$, is compared with the exact angular distribution in Fig. 2. The

TABLE II. Values of the functions $I(\theta)$ and $D(\theta)$ for $Z=47$ and various positron energies. Cross sections are in mb/sr.

$Z=47$	$E=1.25m$		$E=1.50m$		$E=1.75m$	
$\cos\theta$	$I(\theta)$	$D(\theta)$	$I(\theta)$	$D(\theta)$	$I(\theta)$	$D(\theta)$
1.0000	11.562	0.000	20.483	0.000	27.003	0.000
0.9375	9.514	1.836	13.070	1.216	13.718	0.051
0.8750	8.260	2.411	10.329	1.840	10.800	0.805
0.8125	7.407	2.692	8.933	2.082	9.387	1.069
0.7500	6.767	2.807	7.975	2.109	8.254	1.095
0.6875	6.245	2.817	7.190	2.026	7.243	1.023
0.6250	5.795	2.762	6.498	1.893	6.341	0.919
0.5625	5.393	2.667	5.874	1.739	5.547	0.808
0.5000	5.024	2.548	5.309	1.583	4.856	0.702
0.4375	4.684	2.414	4.798	1.431	4.259	0.607
0.3750	4.366	2.275	4.336	1.290	3.743	0.522
0.3125	4.070	2.134	3.921	1.159	3.297	0.449
0.2500	3.792	1.994	3.547	1.040	2.911	0.385
0.1875	3.532	1.858	3.211	0.932	2.576	0.330
0.1250	3.289	1.726	2.908	0.835	2.284	0.282
0.0625	3.061	1.600	2.635	0.747	2.029	0.241
0.0000	2.848	1.480	2.390	0.668	1.805	0.205
−0.0625	2.649	1.366	2.168	0.596	1.608	0.174
−0.1250	2.462	1.257	1.967	0.532	1.434	0.148
−0.1875	2.287	1.155	1.786	0.474	1.280	0.124
−0.2500	2.124	1.057	1.621	0.421	1.144	0.104
−0.3125	1.971	0.965	1.471	0.373	1.022	0.087
−0.3750	1.828	0.877	1.335	0.330	0.913	0.072
−0.4375	1.694	0.794	1.211	0.290	0.816	0.059
−0.5000	1.568	0.714	1.098	0.254	0.728	0.048
−0.5625	1.451	0.637	0.995	0.221	0.650	0.038
−0.6250	1.340	0.563	0.900	0.190	0.578	0.030
−0.6875	1.237	0.491	0.814	0.161	0.514	0.023
−0.7500	1.140	0.420	0.734	0.134	0.456	0.016
−0.8125	1.049	0.347	0.661	0.108	0.403	0.012
−0.8750	0.963	0.271	0.593	0.082	0.355	0.007
−0.9375	0.883	0.183	0.531	0.054	0.311	0.004
−1.0000	0.807	0.000	0.474	0.000	0.271	0.000

TABLE III. Values of the functions $I(\theta)$ and $D(\theta)$ for $Z=73$ and various positron energies. Cross sections are in mb/sr.

$Z=73$	$E=1.25m$		$E=1.50m$		$E=1.75m$	
$\cos\theta$	$I(\theta)$	$D(\theta)$	$I(\theta)$	$D(\theta)$	$I(\theta)$	$D(\theta)$
1.0000	76.842	0.000	189.05	0.00	279.16	0.00
0.9375	64.567	17.176	121.40	26.45	134.52	23.83
0.8750	56.457	22.141	91.41	32.63	91.69	28.77
0.8125	50.640	24.508	75.10	33.98	72.55	28.36
0.7500	46.155	25.464	64.58	33.13	60.90	26.10
0.6875	42.490	25.566	56.88	31.29	52.44	23.38
0.6250	39.363	25.131	50.77	29.06	45.75	20.72
0.5625	36.612	24.360	45.68	26.74	40.25	18.28
0.5000	34.141	23.382	41.33	24.47	35.62	16.11
0.4375	31.890	22.284	37.54	22.32	31.68	14.22
0.3750	29.822	21.123	34.19	20.33	28.29	12.57
0.3125	27.909	19.938	31.23	18.50	25.37	11.13
0.2500	26.133	18.756	28.58	16.83	22.83	9.88
0.1875	24.479	17.592	26.21	15.31	20.61	8.78
0.1250	22.937	16.460	24.08	13.92	18.66	7.81
0.0625	21.496	15.364	22.16	12.66	16.94	6.97
0.0000	20.148	14.309	20.42	11.50	15.42	6.22
−0.0625	18.887	13.296	18.84	10.45	14.07	5.56
−0.1250	17.705	12.326	17.41	9.48	12.86	4.96
−0.1875	16.597	11.398	16.10	8.60	11.78	4.43
−0.2500	15.557	10.509	14.91	7.78	10.81	3.95
−0.3125	14.581	9.657	13.82	7.03	9.93	3.52
−0.3750	13.664	8.839	12.82	6.33	9.14	3.13
−0.4375	12.801	8.052	11.90	5.68	8.43	2.78
−0.5000	11.990	7.292	11.05	5.07	7.78	2.45
−0.5625	11.227	6.554	10.27	4.50	7.18	2.15
−0.6250	10.508	5.832	9.55	3.95	6.64	1.87
−0.6875	9.831	5.119	8.89	3.42	6.15	1.60
−0.7500	9.192	4.404	8.27	2.91	5.70	1.35
−0.8125	8.590	3.670	7.70	2.40	5.28	1.10
−0.8750	8.021	2.884	7.17	1.87	4.90	0.85
−0.9375	7.484	1.964	6.67	1.26	4.54	0.57
−1.0000	6.976	0.000	6.21	0.00	4.22	0.00

TABLE IV. Values of the functions $I(\theta)$ and $D(\theta)$ for $Z=79$ and various positron energies. Cross sections are in mb/sr.

$Z=79$	$E=1.25m$		$E=1.50m$		$E=1.75m$	
$\cos\theta$	$I(\theta)$	$D(\theta)$	$I(\theta)$	$D(\theta)$	$I(\theta)$	$D(\theta)$
1.0000	100.76	0.00	268.30	0.00	407.26	0.00
0.9375	85.54	23.63	175.02	41.13	199.78	40.41
0.8750	75.34	30.52	132.53	50.42	135.63	47.54
0.8125	67.95	33.87	109.04	52.44	106.56	46.52
0.7500	62.18	35.28	93.77	51.18	89.05	42.78
0.6875	57.43	35.51	82.60	48.44	76.55	38.39
0.6250	53.34	34.99	73.77	45.10	66.81	34.12
0.5625	49.73	34.00	66.45	41.61	58.86	30.22
0.5000	46.46	32.71	60.20	38.19	52.21	26.74
0.4375	43.48	31.24	54.77	34.95	46.57	23.69
0.3750	40.73	29.67	49.99	31.93	41.73	21.03
0.3125	38.18	28.06	45.76	29.14	37.55	18.71
0.2500	35.80	26.45	41.98	26.58	33.92	16.68
0.1875	33.59	24.85	38.59	24.25	30.73	14.89
0.1250	31.52	23.29	35.54	22.11	27.93	13.31
0.0625	29.58	21.78	32.78	20.16	25.46	11.92
0.0000	27.76	20.32	30.28	18.37	23.26	10.69
−0.0625	26.05	18.91	28.02	16.73	21.31	9.59
−0.1250	24.45	17.55	25.96	15.22	19.56	8.60
−0.1875	22.95	16.25	24.07	13.84	17.98	7.71
−0.2500	21.54	15.00	22.35	12.55	16.57	6.91
−0.3125	20.21	13.81	20.77	11.37	15.29	6.19
−0.3750	18.96	12.65	19.32	10.26	14.14	5.53
−0.4375	17.78	11.54	17.98	9.23	13.09	4.92
−0.5000	16.67	10.46	16.75	8.26	12.13	4.36
−0.5625	15.63	9.41	15.61	7.34	11.25	3.84
−0.6250	14.64	8.39	14.56	6.46	10.45	3.35
−0.6875	13.71	7.37	13.58	5.62	9.72	2.89
−0.7500	12.83	6.34	12.68	4.79	9.05	2.44
−0.8125	12.00	5.29	11.84	3.96	8.43	2.00
−0.8750	11.22	4.16	11.06	3.08	7.85	1.55
−0.9375	10.48	2.84	10.33	2.08	7.32	1.04
−1.0000	9.77	0.00	9.65	0.00	6.83	0.00

TABLE V. Values of the functions $I(\theta)$ and $D(\theta)$ for $Z=92$ and various positron energies. Cross sections are in mb/sr.

$Z=92$	$E=1.25m$		$E=1.50m$		$E=1.75m$	
$\cos\theta$	$I(\theta)$	$D(\theta)$	$I(\theta)$	$D(\theta)$	$I(\theta)$	$D(\theta)$
1.0000	156.74	0.00	496.40	0.00	800.98	0.00
0.9375	136.37	39.84	337.31	88.28	414.50	100.14
0.8750	122.39	51.94	260.91	108.27	284.42	115.55
0.8125	111.96	58.13	217.00	113.25	223.08	113.09
0.7500	103.61	61.04	187.82	111.36	186.10	104.69
0.6875	96.56	61.90	166.27	106.26	160.10	94.79
0.6250	90.36	61.42	149.18	99.76	140.16	85.06
0.5625	84.78	60.06	134.99	92.78	124.07	76.08
0.5000	79.66	58.12	122.87	85.82	110.70	68.00
0.4375	74.92	55.83	112.32	79.12	99.37	60.85
0.3750	70.50	53.31	103.03	72.80	89.66	54.53
0.3125	66.35	50.66	94.76	66.91	81.26	48.96
0.2500	62.46	47.97	87.36	61.44	73.92	44.03
0.1875	58.80	45.27	80.71	56.40	67.47	39.65
0.1250	55.36	42.61	74.69	51.74	61.77	35.76
0.0625	52.11	39.99	69.24	47.44	56.71	32.30
0.0000	49.04	37.44	64.28	43.48	52.20	29.19
−0.0625	46.15	34.96	59.75	39.81	48.15	26.39
−0.1250	43.43	32.57	55.61	36.42	44.52	23.86
−0.1875	40.85	30.25	51.81	33.27	41.23	21.56
−0.2500	38.42	28.01	48.32	30.34	38.26	19.46
−0.3125	36.12	25.84	45.11	27.60	35.56	17.55
−0.3750	33.95	23.75	42.15	25.03	33.10	15.78
−0.4375	31.90	21.71	39.41	22.61	30.85	14.14
−0.5000	29.96	19.73	36.87	20.32	28.80	12.62
−0.5625	28.12	17.80	34.52	18.14	26.91	11.19
−0.6250	26.38	15.89	32.33	16.04	25.17	9.83
−0.6875	24.74	13.99	30.29	13.99	23.57	8.53
−0.7500	23.18	12.07	28.40	11.98	22.09	7.26
−0.8125	21.70	10.09	26.63	9.93	20.72	5.99
−0.8750	20.30	7.95	24.97	7.77	19.46	4.66
−0.9375	18.97	5.43	23.43	5.27	18.28	3.15
−1.0000	17.71	0.00	21.98	0.00	17.18	0.00

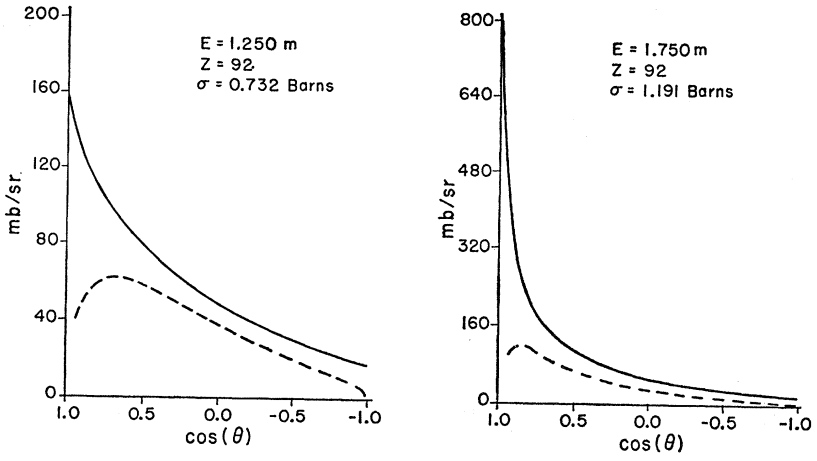

FIG. 5. Angular-distribution functions $I(\theta)$ and asymmetry functions $D(\theta)$ for uranium $Z=92$, at incident positron energies $E=1.25m$ and $1.75m$. The solid curves represent $I(\theta)$ and the dashed curves represent $D(\theta)$.

integrated Born cross section for $Z=92$ and $E=1.5m$ is 4.191 b while the corresponding exact cross section is 1.210 b. We normalize the Born-approximation differential cross section to give the correct total cross section and find that the shapes of the normalized Born angular distribution and exact angular distribution are completely different.

For low values of Z, the numerical program gives angular distributions which agree in shape with the Born approximation. A representation of the differential cross section, accurate for low $Z(\leq 13)$, is obtained by multiplying Eq. (26) by the positron Coulomb normalization factor $\eta e^{-\eta}/\sinh\eta$, with $\eta=\pi\alpha Z/\beta$.

Figure 3 gives angular distributions $I(\theta)$ and asymmetry functions $D(\theta)$ for positron energy $E=1.5m$ and four elements: uranium, $Z=92$; gold, $Z=79$; tantalum, $Z=73$; and silver, $Z=47$. One sees that at this fixed energy the relative magnitude of the asymmetry grows with Z in a roughly linear way. Figures 4 and 5 present the same two functions plotted at energies $1.25m$ and $1.75m$, for gold and uranium, respectively. In Fig. 4 one notices a decrease in $D(\theta)$ at both $1.25m$ and $1.75m$, compared with the value at $1.5m$ given in Fig. 3. This decrease is associated with the fact that the corresponding positron-scattering asymmetry is reduced at these energies.

Numerical values of $I(\theta)$ and $D(\theta)$ are given in Tables II–V, for the four elements mentioned above at energies $E=1.25m$, $E=1.5m$, and $E=1.75m$, and at intervals of $\cos\theta=0.0625$. Using standard interpolation techniques these tables will provide values of the differential cross section and asymmetry function for any target material in the range $47\leq Z\leq 92$, and for any positron energy in the range $1.25m\leq E\leq 1.75m$, to better than 5% accuracy.

The largest corrections to the Coulomb cross sections presented in Tables II–V arise from atomic-screening effects. For the K-shell photoeffect,[15] screening *decreases* total cross sections by several percent, but leaves angular distributions essentially unchanged. Because of the relation of the photoeffect and single-quantum annihilation, we expect screening to *increase* the total cross sections by several percent, and to modify the angular distributions only slightly. The large number of significant figures in Tables II–V are included mainly to facilitate interpolation.

ACKNOWLEDGMENTS

Thanks are due to Dr. Frank Feiock for invaluable assistance with the numerical procedures described in Sec. III. Professor E. Funk and Professor J. Mihelich are to be thanked for discussions concerning the feasibility of measuring the annihilation radiation asymmetry. The author owes an additional debt of graditude to Michael Amoruso for checking the calculations of Sec. II.